AlGaN/GaN Heterostructure Transit-Time Devices: A Novel Device Concept for Submillimeter-Wave Sources

H. Eisele
Institute of Microwaves and Photonics
School of Electronic and Electrical Engineering
University of Leeds, Leeds LS2 9JT, United Kingdom

M. Singh
Research Laboratory of Electronics
Massachusetts Institute of Technology
Cambridge, MA 02139-4307, USA

Y.-R. Wu, J. Singh, and G. I. Haddad
Solid-State Electronics Laboratory
Department of Electrical Engineering and Computer Science
University of Michigan, Ann Arbor, MI 48109-2122, USA

***Abstract*— A novel transit-time device structure for low-noise RF power generation at high millimeter-wave and submillimeter-wave frequencies is proposed. It takes advantage of the unique tunneling properties in strained AlGaN/GaN heterojunctions. The device simulations take realistic heat management for continuous-wave operation on diamond heat sinks into account and, as initial results, predict tunability over a large frequency range and RF power levels (and corresponding dc-to-RF conversion efficiencies) of $>$ 240 mW ($>$ 5%) around 160 GHz and $>$ 15 mW ($>$ 2%) around 320 GHz.**

I. Introduction

A rapidly increasing number of emerging systems applications at submillimeter-wave frequencies, such as imaging, chemical or biological sensing, and wide-bandwidth communications, depends on the availability of compact, reliable, and efficient oscillators [1]. High spectral purity is also a prerequisite when these sources are employed as transmitters or local oscillators (LO) in such applications. Tunneling was recognized as a fast and quiet carrier injection mechanism for transit-time devices in 1958 and the tunnel injection transit-time (TUNNETT) diode was proposed as a millimeter- and submillimeter-wave source [2]. Its operation at submillimeter-wave frequencies was demonstrated first in a pulsed mode [3] and GaAs has been the most commonly used material sytem. Substantial advances in epitaxial growth techniques and refined diode fabrication technologies yielded much improved GaAs TUNNETT diodes whose operation in the continuous-wave (CW) mode was first achieved at V-band (50–75 GHz) and W-band (75–110 GHz) frequencies [4], [5] and, with further improvements in thermal management and oscillator circuits, up to 400 GHz [6]–[9].

Immaterial of the high-frequency properties of the carrier injection mechanism, the carrier drift velocities v_s, dielectric constant ϵ_s, and maximum electric field E_c of the employed semiconductor material system are responsible for the ultimate performance limits of all transit-time devices at high submillimeter-wave frequencies [10]. GaAs as a semiconductor material with direct interband tunneling offers excellent tunneling properties, but its carrier drift velocities, dielectric constant, and breakdown electric field are not so favorable as can be seen from the comparison of relevant semiconductor material properties in Table I.

TABLE I
Properties of Important Semiconductors for RF Power Generation

Property at 300 K	Si	GaAs	InP	6H-SiC (4H-SiC)	GaN	Diamond
Bandgap [eV]	1.12	1.42	1.34	3.06 (3.26)	3.39	5.5
Electron mobility [cm^2/V•s] ⊥ c-axis ‖ c-axis	1400	8500	4600	400 (850) 80 (1020)	900	2200
Hole mobility [cm^2/V•s]	450	400	140	90 (115)	150	1600
Breakdown field at $N_D \approx 10^{17}$ cm^{-3} [MV/cm]	0.61	0.65	0.75	2.5 (2.2)	2	10
Thermal conductivity [W/cm•K]	1.25	0.46	0.68	4.9	1.3	20
Saturated electron drift velocity at $E > 0.5$ MV/cm [$\times 10^7$ cm/s]	1	0.6	0.75	2	1.6	2.7
Dielectric constant	11.8	12.8	12.6	9.7	9	5.5
Electronic P_{RF} figure of merit, relative to Si $(E_c v_s)^2$	1	0.4	0.9	70	25	2000

This table also shows that the relevant material parameters of GaN, including a higher thermal conductivity, are more favorable than those of GaAs. In addition, the wide bandgap of GaN allows higher safe operating temperatures. Current epitaxial growth techniques, however, are unable to produce the p- and n-type doping levels that are sufficiently high for significant interband tunneling.

II. Physics and Properties of GaN/AlGaN Heterojunctions

Different electronegativities of the group III atoms (Ga, Al, etc.) and N atoms cause III-V nitrides to be strongly polar semiconductor materials. The wurtzite crystal structure is common in the epitaxial growth of nitrides like GaN and AlGaN and Table I lists some of the properties of GaN in this crystal structure. III-V nitride heterostructures show the presence of piezoelectric and spontaneous polarization charges at the interface of two different materials [11] (for [0001] growth). This feature is commonly not seen in III-V arsenides grown along the [100] direction and offers a novel method of introducing charges at the interface region of the heterojunction [12]. Such an approach frees device designers from some of the limitations involved in doping wide bandgap semiconductors. Tunneling transport across III-V heterojunction diodes has been studied before [13] and these studies revealed good agreement with experimentally observed contact resistance values [14].

The case of an $Al_xGa_{1-x}N$ epitaxial layer grown on a GaN substrate is considered here. The total polarization charge $P(x)$ depends on the Al composition x and has the value [15]

$$\begin{aligned} P(x) &= P_{pz} + P_{sp} \\ &= (-3.2 \times x - 1.9x^2) \times 10^{-6}\ \mathrm{C/cm^2} \\ &\quad -5.2 \times 10^{-6} x\ \mathrm{C/cm^2} \end{aligned} \tag{1}$$

In this system, the effects arising from the piezoelectric effect P_{pz} and the spontaneous polarization mismatch P_{sp} are comparable. However, these two effects may have opposite directions depending on the surface termination conditions and the lattice mismatch between the epitaxial layer and the effective substrate. Because of better crystal morphology, Ga-faced growth is preferred to N-faced growth in most cases and results in the same directions of both effects.

The tunneling transport across the barrier is very sensitive to the composition of the $Al_xGa_{1-x}N$ barrier layer as well as its thickness. For small thicknesses, the probability of tunneling through the barrier is high, but the charge control model shows that there is very little carrier population in the two-dimensional electron gas (2DEG). In this case, there are no allowed 2DEG states for electrons to tunnel to from the metal and, as a result, the tunnel current is supported by a final three-dimensional density of states. For large thicknesses, the number of available states is increased, but the Wenzel-Kramers-Brillouin (WKB) tunneling probability is suppressed. This corresponds to a trade-off situation where the tunneling current needs to be optimized. In the intermediate range, the barrier thickness is large enough to allow the existence of a sizable 2DEG and small enough to allow tunneling through the barrier.

III. Device Simulations

A. Device structure and simulation method

Figure 1 shows the schematic structure of the proposed device. This structure consists of a Schottky contact and the AlGaN/GaN heterojunction as the tunnel injection region. The subsequent n-type doping spike reduces the electric field from values of more than 3 MV/cm at the heterojunction to values of 100–500 KV/cm for electrons (and holes) in the drift region to travel at the highest possible drift velocities. The wide bandgap of GaN makes the formation of excellent ohmic contacts rather difficult. Ohmic contacts with very low contact resistances have been reported [14]–[18], but they are not considered as fully compatible with the envisaged device fabrication technologies. Therefore, a second Schottky contact on the n-type contact region is used instead [19], [20]. Its voltage drop is small compared to the applied bias voltages of more than 12 V and its equivalent contact resistance drops well below $1 \times 10^{-6}\ \Omega\mathrm{cm}^2$ for the applied current densities of more than 50 kA/cm^2.

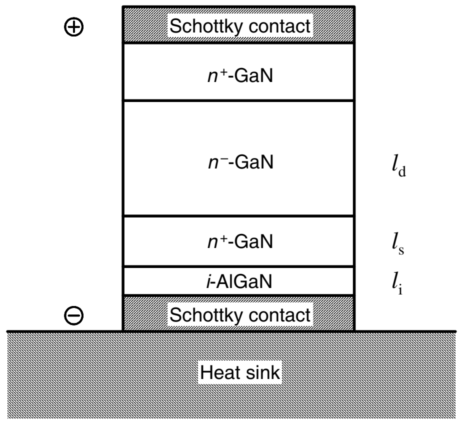

Fig. 1. Schematic structure of the AlGaN/GaN heterojunction transit-time device.

Solving the time-dependent Schrödinger equation for the complete device structure is too computing intensive. Tunneling is much faster when compared with the RF cycles that are considered in this paper. Therefore, the simulation runs for the RF performance predictions are split into two parts. One program considers the tunneling process and determines the quasi-static current-voltage characteristics of the AlGaN/GaN heterojunction. These characteristics are then converted to field-dependent current densities at the location of the heterojunction interface. The subsequent runs of the other program with the hydrodynamic device model [21] use these injection current densities as a variable boundary condition and take the complete doping profile of the device into account. This program determines the device impedance, RF output power, dc-to-RF conversion efficiency, and operating junction temperature as a function of the operating frequency.

B. Band-structure and tunneling calculations

Details of the model have been published earlier [12], [13], [22]. Essentially it involves the following two steps:

- Self-consistent solution of the Schrödinger and Poisson equations to obtain the wavefunctions and energies for the carriers in the heterostructure as well as the shape of the conduction band;

- Use of the quantities obtained above to calculate the Wenzel-Kramers-Brillouin tunneling probability at each energy.

The tunneling current can then be calculated [13]. The results for a device structure with an $Al_{0.3}Ga_{0.7}N/GaN$ heterojunction are shown in Fig. 2(a), while the results for an $Al_{0.15}Ga_{0.85}N/GaN$ heterojunction are shown in Fig. 2(b), both assuming an active-layer temperature of 600 K. The higher Al composition of 30% is used in the device because better band alignment yields a higher reverse bias current.

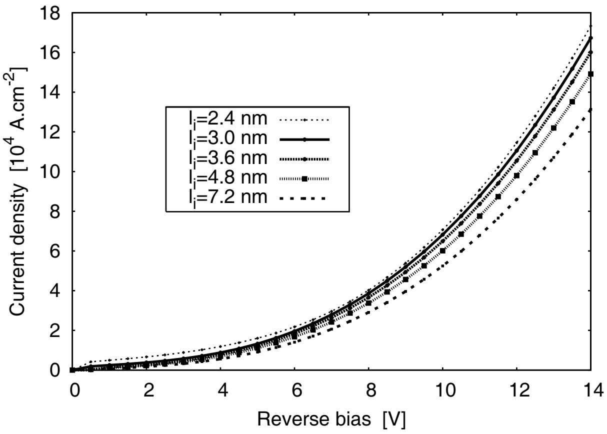

(a) $Al_{0.3}Ga_{0.7}N/GaN$, T = 600 K

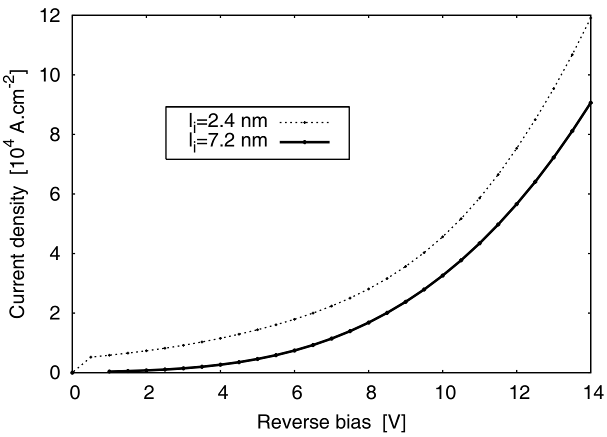

(b) $Al_{0.15}Ga_{0.85}N/GaN$, T = 600 K

Fig. 2. Reverse-bias tunnel current for two Al compositions x and different thicknesses l_i of the $Al_xGa_{1-x}N$ layer.

C. RF simulations

The hydrodynamic model uses material parameters of GaN which were taken from published results of Monte Carlo simulations [23], [24] and experiments [25]. Impact ionization was found to play an insignificant role in this device. However, it is taken into account in the simulation program with appropriate rates for GaN [26].

Thermal management with proper heat sinks critically affects the performance of all fundamental solid-state sources at millimeter- and submillimeter-wave frequencies. Diamond is the material with best thermal properties above 200 K and is the first choice for such a heat sink. Realistic device simulations need to take the influence of the heat sink, that is, the substantial temperature rise inside the heat sink, properly into account. The importance of this can be seen with the IMPATT diode of [27], which actually operates in the CW mode at much higher junction temperatures than 600 K as assumed in that paper. The spreading approximation [28] predicts the thermal resistance of mesa-type two-terminal devices and has yielded excellent agreement with measurements on Si and GaAs IMPATT diodes as well as GaAs and InP Gunn devices since its inception more than two decades ago. This approximation method predicts that the junction temperature of the diode with the area of 1×10^{-6} cm^2 exceeds 2000 K at the bias voltage and current of 50 V and 300 mA [27], respectively, when a diamond heat sink with a typical metalization scheme and a thermal conductivity at 500 K of 11 W/cmK are assumed.

Table II lists the device parameters and bias conditions that have resulted in the best performance so far around the two center frequencies considered in this paper. The thickness of the $Al_{0.3}Ga_{0.7}N$ layer was kept at 4.8 nm. As can be seen from Fig. 2(a), this thickness meets the requirements for efficient device operation: the injected tunneling current is very small at reverse bias voltages below 3 V and rapidly reaches current densities of more than 50 kA/cm^2 at reverse bias voltages of more than 5 V, thus ensuring a sharp turn-on of the carrier injection during the RF cycle.

During the RF simulation runs, the bias current densities were adjusted such that the operating junction temperatures of devices in the CW mode on diamond heat sinks remained below 600 K. To maintain the same load conditions for comparison purposes, the real part of the load impedance, $\underline{Z}_L = R_L + jX_L$, was kept fixed at 1 Ω and the device area at different frequencies adjusted accordingly.

Fig. 3 compares the predicted heat flow resistances of the AlGaN/GaN heterostructure transit-time devices with those of the aforementioned GaAs TUNNETT diodes [6], [29]. The GaN-based devices show much lower heat flow resistances, in particular for device diameters below 25 μm as used in the simulations. Lower heat flow resistances and higher permissible active-layer operating temperatures allow the devices to be operated at dc input power levels higher than those of GaAs TUNNETT diodes. Therefore, much higher RF output power levels are generated.

IV. Results

Fig. 4 shows the RF power levels and corresponding dc-to-RF conversion efficiencies for device structure 1 designed for a center operating frequency of 160 GHz and for a specific contact resistance of 1×10^{-6} Ωcm^2. The device generates more than 240 mW around the design frequency and more than 150 mW over a wide frequency range of 135–200 GHz, which makes the devices well suited for tunable sources in an oscillator circuit with a wide tuning range. The dc input power consumption is less

TABLE II

DEVICE PARAMETERS

Parameter	Structure 1	Structure 2
$f_{\rm design}$ [GHz]	160	320
$l_{\rm i}$ [nm]	4.8	4.8
$l_{\rm s}$ [nm]	54	54
$l_{\rm d}$ [nm]	545	245
$N_{\rm s}$ [$\times 10^{16}$/cm^2]	130	160
$N_{\rm d}$ [$\times 10^{16}$/cm^2]	3	4.5
$J_{\rm DC}$ [kA/cm^2]	55	80
$V_{\rm DC}$ [V]	24	14

than 5 W, which allows the device to be used in portable systems applications.

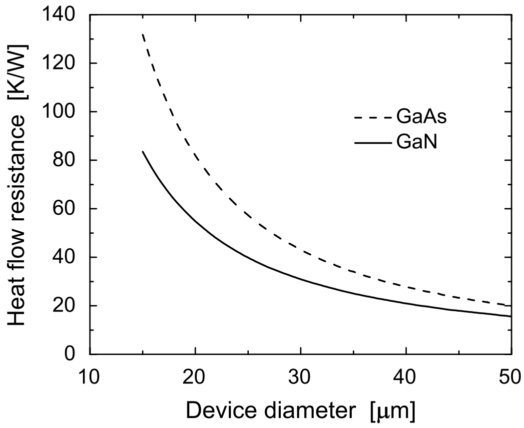

Fig. 3. Predicted heat flow resistances of GaAs and GaN devices on diamond heat sinks

Device structure 2 operates at a higher current density and, therefore, the simulation results of Fig. 5 are based on a lower specific contact resistance of 5×10^{-7} Ωcm^2. Similar to structure 1, the device operates over a wide frequency range with more than 12 mW at 280–380 GHz. The device generates more than 15 mW around the design frequency of 320 GHz. With a bias voltage of less than 14 V and a total dc input power consumption of less than 0.9 W, this device is well suited for battery-operated systems applications.

V. CONCLUSIONS

A novel device structure for low-noise power generation at millimeter- and submillimeter-wave frequencies was proposed and simulated in two frequency ranges around 160 GHz and 320 GHz. The predictions take realistic contact resistances and heat sink properties into account. The predicted RF power levels compare favorably with those from other two-terminal devices in the same frequency range. More importantly, the proposed device structure offers much higher dc-to-RF conversion efficiencies than

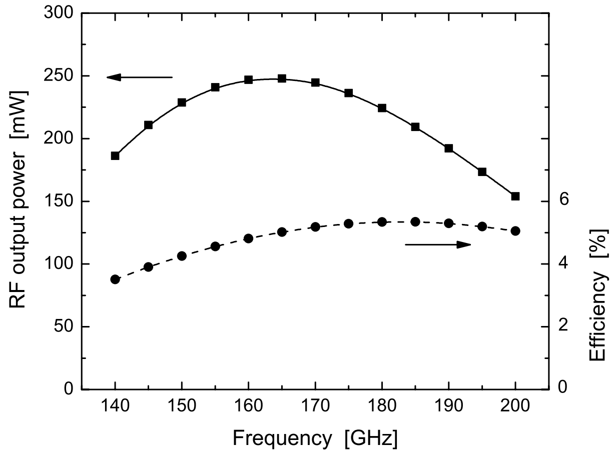

Fig. 4. Predicted RF performance of structure 1

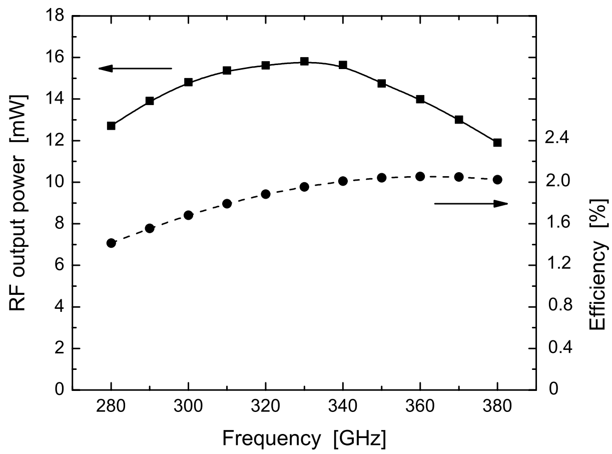

Fig. 5. Predicted RF performance of structure 2

those predicted for other two-terminal devices in the same frequency range.

Additional fine-tuning of the doping profiles and heterojunction parameters is expected to improve the RF performance even further. However, significant advances in device fabrication technologies for GaN-based devices similar to those established for GaAs- and InP-based devices are prerequisites before the potential of these novel devices can be harnessed.

This type of device is also expected to generate signficant amounts of RF power at much higher submillimeter-wave frequencies, but additional relaxation time constants need to be taken into account in the simulation model to obtain realistic performance predictions and optimum device designs.

REFERENCES

[1] P. Siegel, "Terahertz technology," *IEEE Trans. Microwave Theory Tech.*, vol. 50, pp. 910–928, 2002.

[2] J. Nishizawa and Y. Watanabe, "High frequency properties of the avalanching negative resistance diode," Research Institute Tohoku University, Tech. Rep., 1958.

[3] J. Nishizawa, K. Motoya, and Y. Okuno, "Submillimeter-wave oscillation from GaAs TUNNETT diode," in *Proc. 9^{th} European Microwave Conf.*, Sept. 17–20, 1979, pp. 464–467, Brighton, UK.

[4] M. Pöbl, C. Dalle, and W. Harth, "CW mm-wave GaAs TUNNETT diode," *Electron. Lett.*, vol. 26, pp. 1540–1542, 1990.

[5] C. Kidner, H. Eisele, and G. I. Haddad, "Tunnel injection transit-time diodes for W-band power generation," *Electron. Lett.*, vol. 28, no. 5, pp. 511–513, 1998.

[6] H. Eisele, A. Rydberg, and G. I. Haddad, "Recent advances in the performance of InP Gunn devices and GaAs TUNNETT diodes for the 100–300 GHz frequency range and above," *IEEE Trans. Microwave Theory Techniques*, vol. 48, no. 4, pp. 626–631, April 2000.

[7] P. Płotka, J-i. Nishizawa, T. Kurabayashi, and H. Makabe, "240-325-GHz GaAs CW Fundamental-Mode TUNNETT Diodes Fabricated With Molecular Layer Epitaxy," *IEEE Trans. Electron Devices*, vol. 50, no. 4, pp. 867–873, April 2003.

[8] H. Eisele, "355 GHz oscillator with GaAs TUNNETT diode," *Electron. Lett.*, vol. 41, no. 6, pp. 329–331, March 2005.

[9] J-i. Nishizawa, P. Płotka, H. Makabe, and T. Kurabayashi, "290-393-GHz CW fundamental-mode oscillation from GaAs TUNNETT diode," *Electron. Lett.*, vol. 41, no. 7, pp. 80–81, March 2005.

[10] G. I. Haddad, J. East, and H. Eisele, "Two-terminal active devices for terahertz sources," in *Vol I: Electronic Devices and Advanced Systems Technology*, ser. Terahertz Sensing Technology, D. Woolard, M. S. Shur, and W. Leorop, Eds. Singapore: World Scientific Publishing, 2003, pp. 45–77.

[11] O. Ambacher, J. Smart, J. R. Shealy, N. G. Weimann, K. Chu, M. Murphy, W. J. Schaff, L. F. Eastman, R. Dimitrov, L. Wittmer, M. Stutzmann, W. Rieger, and J. Hilsenbeck, "Two-dimensional electron gases induced by spontaneous and piezoelectric polarization charges in N- and Ga-face AlGaN/GaN heterostructures," *J. Appl. Phys.*, vol. 85, pp. 3222–3233, 1999.

[12] M. Singh, Y. Zhang, J. Singh, and U. Mishra, "Examination of tunnel junctions in the AlGaN/GaN system: consequences of polarization charge," *Appl. Phys. Lett.*, vol. 77, no. 12, pp. 1867–1869, 2000.

[13] M. Singh, J. Singh, and U. Mishra, "Current-voltage characteristics of polar heterostructure junctions," *J. Appl. Phys.*, vol. 91, no. 5, pp. 2989–2993, March 2002.

[14] D. Qiao, L. Jia, L. S. Yu, P. M. Asbeck, S. S. Lau, S. H. Lim, Z. Liliental-Weber, T. E. Haynes, and J. B. Barner, "Ta-based interface ohmic contacts to AlGaN/GaN heterostructures," *J. Appl. Phys.*, vol. 89, no. 10, pp. 5543–5546, 2001.

[15] I. P. Smorchkova, C. R. Elsass, J. P. Ibbetson, R. Ventury, B. Heying, P. Fini, E. Haus, S. P. DenBaars, J. S. Speck, and U. K. Mishra, "Polarization-induced charge and electron mobility in AlGaN/GaN heterostructures grown by plasma-assisted molecular-beam epitaxy," *J. Appl. Phys.*, vol. 86, no. 8, pp. 4520–4526, 1999.

[16] Z. Fan, S. N. Mohammad, W. Kim, O. Aktas, A. E. Botchkarev, and H. Morko, "Very low resistance ohmic contacts to n-GaN," *Appl. Phys. Lett.*, vol. 68, no. 12, pp. 1672–1674, 1996.

[17] J. Burm, K. Chu, W. A. Davis, W. J. Schaff, L. F. Eastmann, and T. J. Eustis, "Ultra-low resistive ohmic contacts on n-GaN using Si implantation," *Appl. Phys. Lett.*, vol. 70, no. 4, pp. 464–466, Jan. 1997.

[18] S. J. Cai, R. Li, Y. L. Chen, L. Wong, W. G. Wu, S. G. Thomas, and K. L. Wang, "High performance AlGaN/GaN HEMT with improved ohmic contacts," *Electron. Lett.*, vol. 34, no. 24, pp. 2354–2356, Nov. 1998.

[19] Y. Konishi, S. T. Allen, M. Reddy, and M. J. W. Rodwell, "AlAs/GaAs Schottky-Collector Resonant-Tunnel-Diodes," *Solid-State Electron.*, vol. 36, no. 12, pp. 1673–1676, 1993.

[20] M. Tschernitz and J. Freyer, "140 GHz GaAs double-Read IMPATT diodes," *Electron. Lett.*, vol. 31, no. 7, pp. 582–583, 1995.

[21] C.-C. Chen, R. K. Mains, G. I. Haddad, and H. Eisele, "Numerical simulation of TUNNETT and MITATT devices in the millimeter and submillimeter range," in *Proc. 4^{th} Int. Symp. Space Terahertz Technology*, Los Angeles, CA, March 30 - April 1, 1993, pp. 362–376.

[22] Y.-R. Wu, M. Singh, and J. Singh, "Gate leakage suppression and contact engineering in nitride heterostructures," *J. Appl. Phys.*, vol. 94, no. 9, pp. 5826–5831, 2003.

[23] J. Kolník, Í. H. Oğuzman, K. F. Brennan, R. Wang, P. P. Ruden, and Y. Wang, "Electronic transport studies of bulk zincblende and wurtzite phases of GaN based on an ensemble Monte Carlo calculation including a full zone band structure," *J. Appl. Phys.*, vol. 78, no. 2, pp. 1033–1038, July 1995.

[24] J. D. Albrecht, R. P. Wang, P. P. Ruden, M. Farahmand, and K. F. Brennan, "Electron transport characteristics of GaN for high temperature device modeling," *J. Appl. Phys.*, vol. 83, no. 9, pp. 4777–4781, May 1998.

[25] M. Wraback, H. Shen, J. C. Carrano, T. Li, J. C. Campbell, M. J. Schurman, and I. T. Ferguson, "Time-resolved electroabsorption measurement of the electron velocity-field characteristic in GaN," *Appl. Phys. Lett.*, vol. 76, no. 9, pp. 1155–1157, Feb. 2000.

[26] J. Kolník, Í. H. Oğuzman, K. F. Brennan, R. Wang, and P. P. Ruden, "Monte Carlo calculation of electron initiated impact ionization in bulk zinc-blende and wurtzite GaN," *J. Appl. Phys.*, vol. 81, no. 2, pp. 726–733, Jan. 1997.

[27] A. Reklaitis and L. Reggiani, "Monte-Carlo study of hot-carrier transport in bulk wurtzite GaN and modeling of a near-terahertz impact avalanche transit-time diode," *J. Appl. Phys.*, vol. 95, no. 12, pp. 7925–7935, 2004.

[28] L. H. Holway and M. G. Adlerstein, "Approximate formulas for the thermal resistance of IMPATT diodes compared with computer calculations," *IEEE Trans. Electron Devices*, vol. 24, pp. 156–159, 1977.

[29] H. Eisele and G. I. Haddad, "Enhanced performance in GaAs TUNNETT diode oscillators above 100 GHz through diamond heat sinking and power combining," *IEEE Trans. Microwave Theory Tech.*, vol. 42, no. 12, pp. 2498–2503, Dec. 1994.